Chapter 8

Effect of Dielectric in a Plasma Annealing System at Atmospheric Pressure

N.D. Tran , N. Harada, T. Sasaki and T. Kikuchi

Additional information is available at the end of the chapter

http://dx.doi.org/10.5772/50594

1. Introduction

Thin metallic wire is widely used in electrical, electronic and automobile technology. It is, however, necessary to anneal and clean the copper wire after drawing. The traditional manufacturing process of fine wire consists of three processes: drawing, annealing and cleaning as shown in Figure 1 and 2 [1]. These processes use Joule heating and chemicals to anneal and clean the wire [2-4]. However, this method has some drawbacks: low efficiency due to the division of the annealing and cleaning processes and environmentally harmful because of using chemical to clean thin wire, for example, Tri-chloethane, it is hazardous to human body and has ozone layer effect. The new annealing system in which the annealing and cleaning processes are simultaneously operated in Atmospheric Pressure Dielectric-Barrier Discharge (APDBD) [5-9] is the potential solution for these drawbacks. In previous studied, it is shown that wire annealing [10, 11] and cleaning [12] using APDBD is totally possible. Also, our previous studies showed that annealing using APDBD is possible for thin copper wire [13], [14] however; the annealing efficiency is low due to choosing the material, size and shape of the dielectric, discharge gas, applied power,... In this study, the efficiency of dielectric material on the annealing and cleaning results was investigated. It is, however, the dielectric material and the dielectric size are the first two important parameters need to be investigated. Moreover, the efficiency of the frequency and the applied voltage of the applied power in the dielectric permittivity were also investigated. To clarify these dependences, an equivalent circuit model is used to analyze the effect of dielectric.

1.1. Annealing

Based on Kalpakjian's Manufacturing Engineering and Technology, annealing is a general term used to describe the restoration of a cold-worked or heat-treated metal or alloy to its original properties, such as to increase elongation rate and reduce hardness and strength, or

to modify the microstructure. The traditional thin metallic wire annealing is using external heating source or Joule heating as shown in Figure 2.

The purpose of annealing thin metallic wire is using heat to increase elongation rate in short duration. The temperature and duration of annealing affect the crystal size and crystal texture of thin wire. And elongation rate depends on the size and orientation of crystal. In addition, the annealing temperature is configured by drawing process; generally lower than 2/3 melting point of the wire material. With assuming that the drawing process is stable then deformation degree is constant. Therefore, in order to reach the required elongation rate, the temperature, and duration of annealing need to be properly chosen.

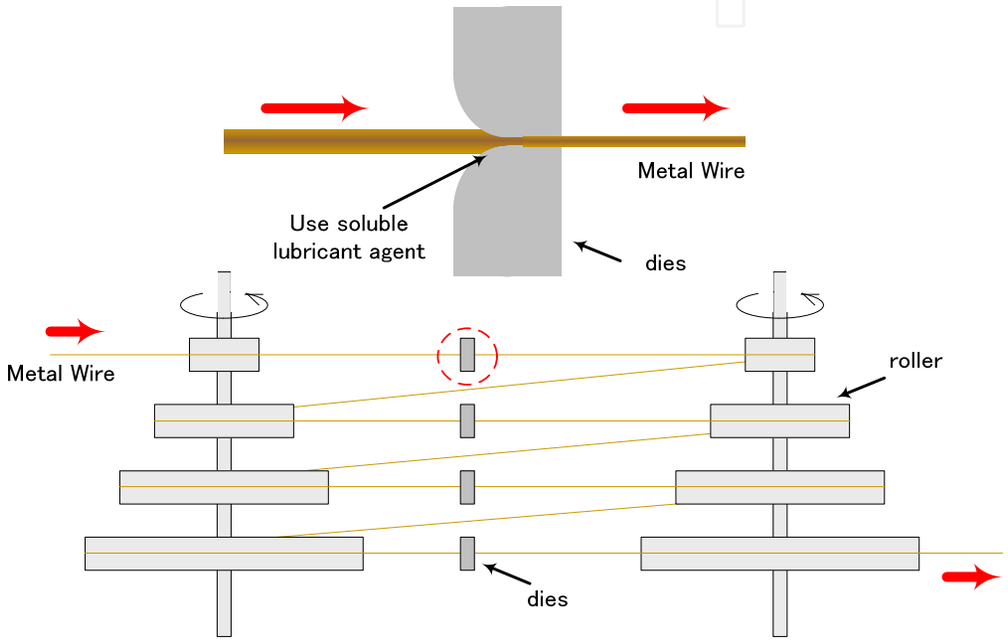

Figure 1. Mechanism of drawing process

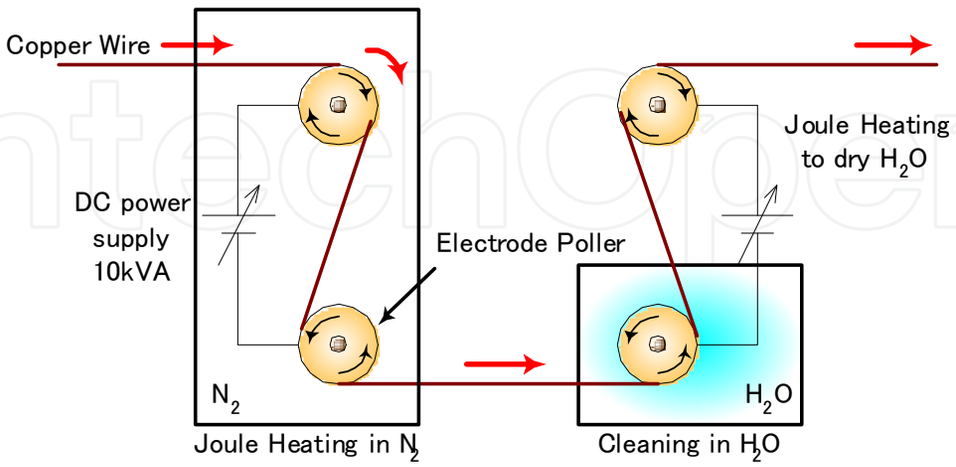

Figure 2. Traditional mechanism of annealing and cleaning process

Heating thin metallic wire at annealing temperature is a thermodynamic process, which is used to rearrange or eliminate of dislocations (recovery), create new crystal (primary

recrystallization) and grow crystal (recrystallization). After annealing, if the crystal size is enlarged and in good orientation, the elongation rate increases. At the first state, the recovery process, some the crystals are not fully rearranged therefore the elongation rate is still low. At primary recrystallization process, a number of crystals in the wire are born and this process strongly depends on the temperature but not duration. However, when the temperature is so high, the number of formed crystal increases then crystal size is small. Small size crystal means elongation rate is low. Therefore, choosing temperature in this process is important to get good orientation of crystal. At the recrystallization process, the crystals were born from the previous process will grow up. The crystal growth depends on duration. No noteworthy crystal growth will occur in the short annealing period then crystal size remains the same. Therefore, the duration of annealing in this process is important to get good orientation of crystal. For continuously thin wire annealing, to have good period annealing, applied voltage and the velocity of thin wire moved through or the length of chamber along the thin wire of plasma reactor have to be considered. If annealing duration is long, the annealing temperature at the end of the process is high and it is the cause of some disadvantages like increasing surface roughness. Moreover, during annealing at high temperature, the presence of hydrogen in air can increase the roughening effect of thin wire.

1.2. Plasma annealing

In order to solve the environmental harm of traditional annealing method, the plasma annealing is replaced. At low pressure such as in vacuum, the temperature generated by the ion bombarding on a target was studied for using in plasma immersion ion implantation (PIII) [15, 16]. This phenomenon was generally applied in modifying the target surface [16, 17] or heating the target [18, 19]. However, these systems operate under expensive vacuum systems. Recently, the atmospheric pressure dielectric barrier discharge (APDBD) for wire annealing has become greatly interesting [20, 21] because of its low-cost system and being environmentally friendly.

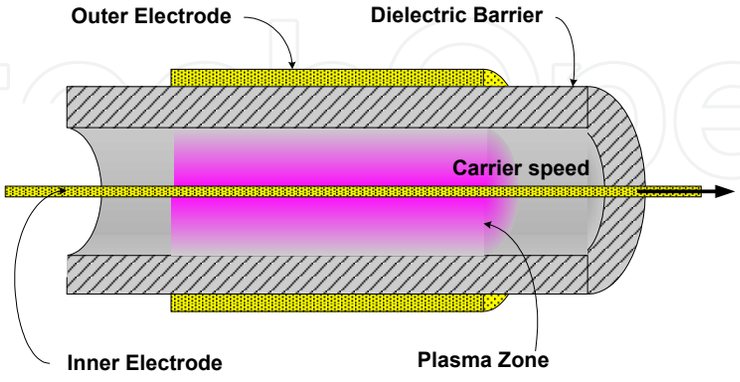

Figure 3. Annealing thin wire at atmospheric pressure dielectric barrier discharge

At atmospheric pressure dielectric barrier discharge, the thin metallic wire is annealed by moved through the plasma reactor as shown in Figure 3. The dielectric is used to prevent the arc and the gas is fed into reactor to assist plasma discharge. The conceptual layout of

plasma annealing is shown in Figure 4. In the plasma reactor, the discharge gas is ionized into electron and ion. Under a strong electric field, ion and electron bombard the thin wire surface. The essence of the generated temperature is the impact energy of electrons and ions on thin wire surface as shown in Figure 5. Furthermore, the electron-neutral particle collisions in streamers also assist generating temperature. The total temperature generated by the charged particle bombarding (ions and electrons) and the electron-neutral collision continuously heats the wire surface to annealing temperature.

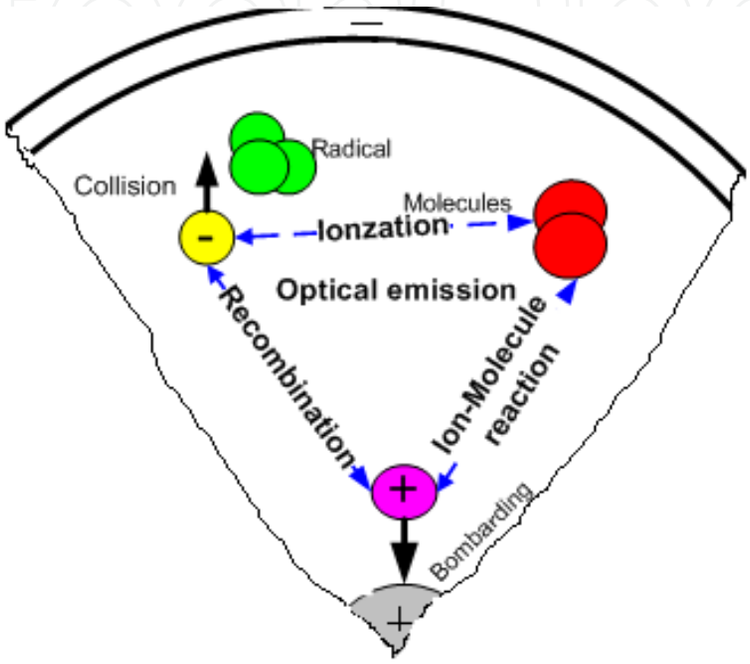

Figure 4. Plasma annealing phenomenon

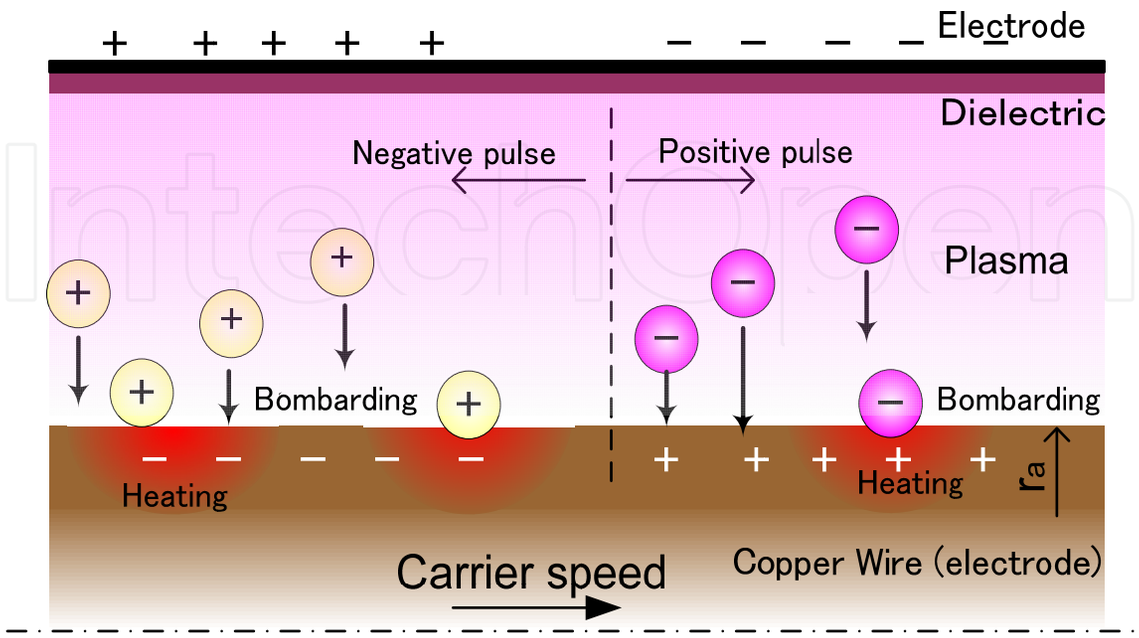

Figure 5. Annealing mechanism

1.2.1. Electron bombarding

Electron bombarding on the target was studied for melting target [22-25]. The electrons bombard the anode (thin wire) and then convert their kinetic energy into thermal energy. Heat transfer occurs from the plasma to the anode in several ways. Firstly, the electrons have thermal energy, which they release upon contact with the anode. Secondly, the electrons also have kinetic energy, which partially gets converted to thermal energy as it passes through the anode. It is important to note that the transfer kinetic energy from electron to anode depends on the current density.

1.2.2. Ion bombarding

The ion bombarding on a target was studied for using in plasma immersion ion implantation (PIII) [15, 16]. When the negative high-voltage pulse is applied to the target, the electrons near the cathode are driven away on the time scale of inverse electron plasma frequency, which is relatively shorter than the time scale of inverse ion plasma frequency, leaving the ions behind to form an ionic space charge sheath. On the time scale of inverse ion plasma frequency, the ions within this sheath are accelerated and then bombard the target surface under the sheath electric field. This phenomenon was generally applied in modifying the target surface [16, 17] or heating the target [17, 18] using low-pressure plasma. It is known that the treatment effect depends on ion bombarding energy, i.e., sheath thickness, ion current, and sheath electric field. On the basis of the fluid model [26] or kinetic model [27-29], it is possible to calculate dynamic sheath thickness, ion current, or ion bombarding energy. Recently, the atmospheric pressure dielectric barrier discharge (APDBD) for annealing thin wire has become greatly interesting [21, 30]. Also, our previous studies showed that annealing using APDBD is possible for thin copper wire [31]. However, the generated temperature by ion bombarding was not estimated. In this study, an analysis model using helium, argon or nitrogen gases and low-frequency (35 – 45 kHz) applied voltage is proposed to analyze the annealing result in APDBD.

2. Experiment setup

The system consists of a gas tank, a power supply, a plasma reactor, a spectrometer sensor and a temperature sensor, as shown in Figure 6. The connecting power to the cylindrical reactor is shown in Figure 7. The design parameters of the reactor shown in Figure 8 are shown in Table 1. The thin cylindrical aluminum electrode (outer electrode) is covered with a dielectric to prevent arcing and it is connected to a power supply (20 kVp-p, 2 Ap-p, and 45 kHz). The thin copper wire (inner electrode) is driven through the reactor by carriers and connected to the ground. Before annealing, the reactor is filled up with discharge gas; helium, argon or nitrogen (purity > 99.9%). During annealing, purified discharge gas is continuously fed into the plasma reactor under a control flow rate to assist the plasma discharge. The applied voltage and current waveform are recorded using a digital oscilloscope (Yokogawa SL1000) with a high voltage probe (Iwatsu HV-P30), and a Rogowski coil (PEARSONTM current monitor 4997), respectively. The elongation rate of

three samples is measured by SAIKAWA ET-100. The industrial required elongation rate is higher 20%.

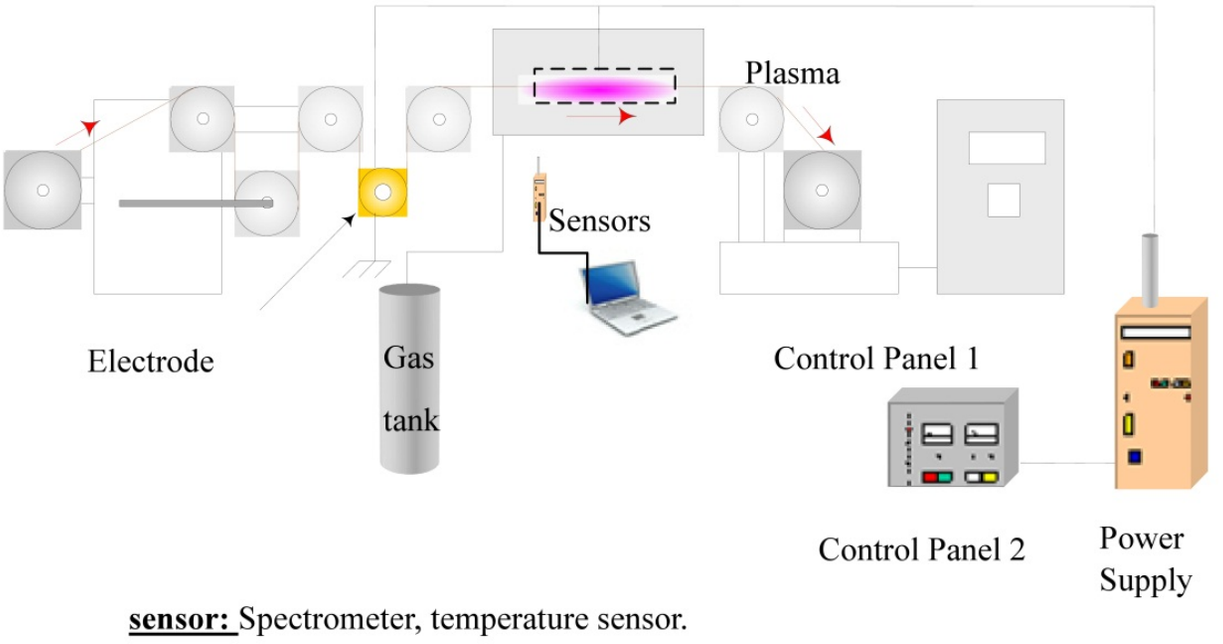

Figure 6. The schematic diagram of the thin wire plasma annealing system

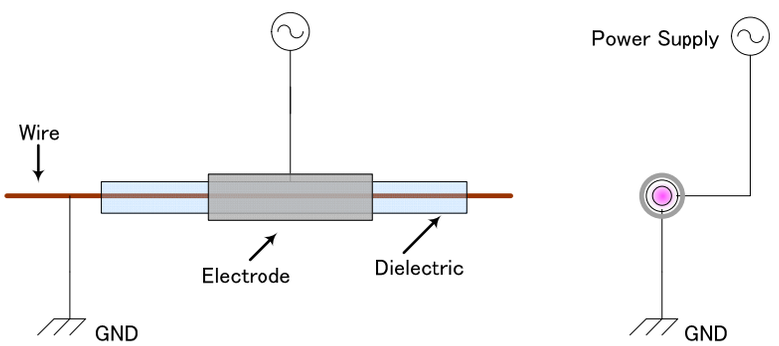

Figure 7. Cylindrical DBD reactor

Diameter of copper wire (mm)	0.2
Dielectric thickness (mm)	2.5
Dielectric material	Glass
Gap length (mm)	4.9
Reactor length (mm)	100
Gas	Ar/He/N2
Gas mass low (l/min)	5
Applied voltage frequency (kHz)	45
Velocity of copper wire (m/min)	30

Table 1. Experimental setup parameters

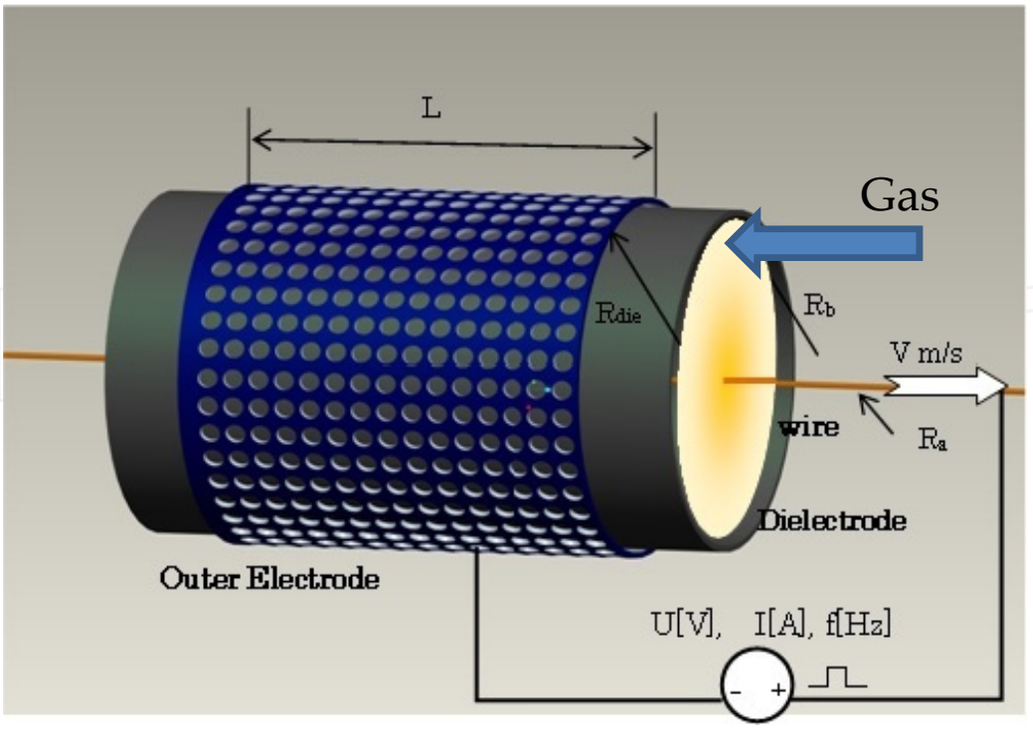

Figure 8. Cylindrical DBD reactor with design parameters

Temperature range	300 °C～1000 °C
Accuracy	0.5% of measurement value +1°
Responding time	2ms
Distance and area measurement	88mm/ϕ0.45～4500mm/ϕ22

Table 2. IGAR12-LO MB10's specifications parameters.

3. Results and discussions

3.1. Dielectric permittivity measurement

The dependence of the dielectric permittivity on the frequency in APDBD annealing system is measured by electrode contact and CLR as shown in Figure 9. Dielectric material is placed sandwich in two aluminum electrodes, high voltage, high frequency function generator is used as power supply. Table 3 shows the experiment equipment be used in this study.

As shown in Figure 9, the dependence of dielectric permittivity on the dielectric voltage V is expressed via capacitance C as

$$V = \frac{I}{j \cdot \omega \cdot C} \tag{1}$$

where parallel capacitor C is expressed by

$$C = \frac{\varepsilon_r \cdot \varepsilon_0 \cdot S}{d}, \tag{2}$$

where S is area of dielectric, d is discharge gap, ε_r and ε_0 is the dielectric and free-space permittivity, respectively. From equation (1) and (2) the dielectric permittivity (3) can be expressed as

$$\varepsilon_r = \frac{d}{\varepsilon_0 \cdot S} \cdot \frac{I}{\omega} \cdot \frac{1}{V}. \tag{3}$$

For comparison, the CRL meter also is used to measure the dielectric permittivity as shown in Figure 9.

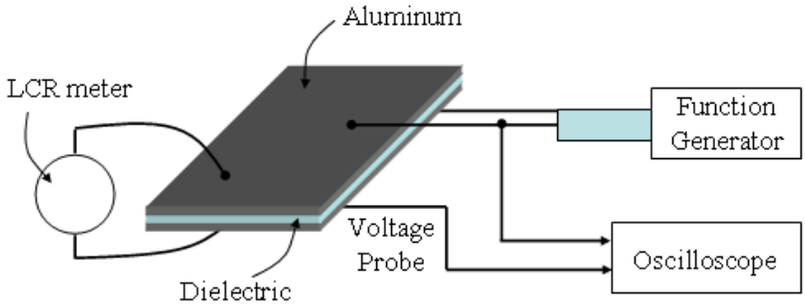

Figure 9. The schematic diagram of the dielectric permittivity measurement

From equation (3), the dependence of dielectric permittivity on frequency was shown in Figure 10. The results show that the dielectric permittivity in the APDBD decreases when frequency increases. At 45kHz, the dielectric permittivity of BN and Al_2O_3 are 12.9 and 6.79, respectively. Moreover, Table 4 shows the comparison of the dielectric permittivity at three measurement methods; our analysis, LCR, and literature. The results also show that at low frequency, the dielectric permittivity is higher than that literature however, at high frequency they are nearly the same.

Function generation	NF Corporation model WF1973
Oscilloscope	Agilent Technologies DSO 1024A
High voltage probe	Agilent Technologies N 2863A
LCR meter	Agilent Technologies Ul732A

Table 3. Equipment used

Frequency f [kHz]	Dielectric permittivity ε_r					
	Electrode contact		LCR		Literature [20, 21]	
	BN	Al_2O_3	BN	Al_2O_3	BN	Al_2O_3
1			5.95	4.82	6.8*	8.1
10	31.7	22.9	4.95	4.76		
45	12.9	6.79				
100	7.19	5.46	7.83	5.12		

Table 4. Comparison dielectric permittivity between measurement and literature

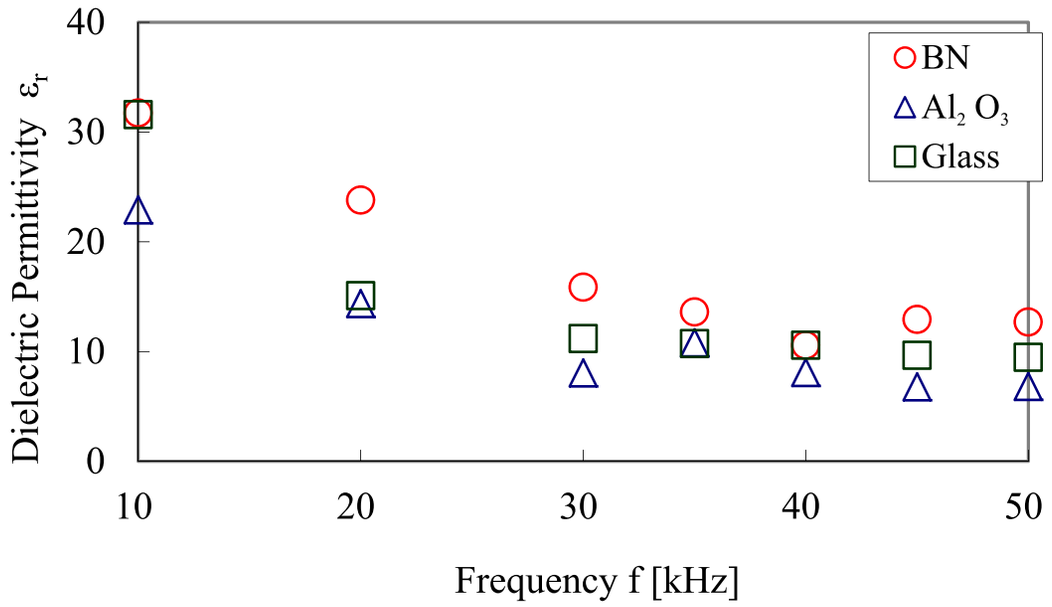

Figure 10. Dependency of dielectric permittivity on frequency

3.2. Dependence of annealing temperature on frequency

Figure 11 shows the experiment result, the dependence of elongation rate on frequency. The result shows the weakly positive relation between the elongation rate and the input frequency. When the frequency increases from 30 kHz to 40 kHz, the elongation rate slightly increases. Thus, we estimate that frequency has no effect on the annealing temperature.

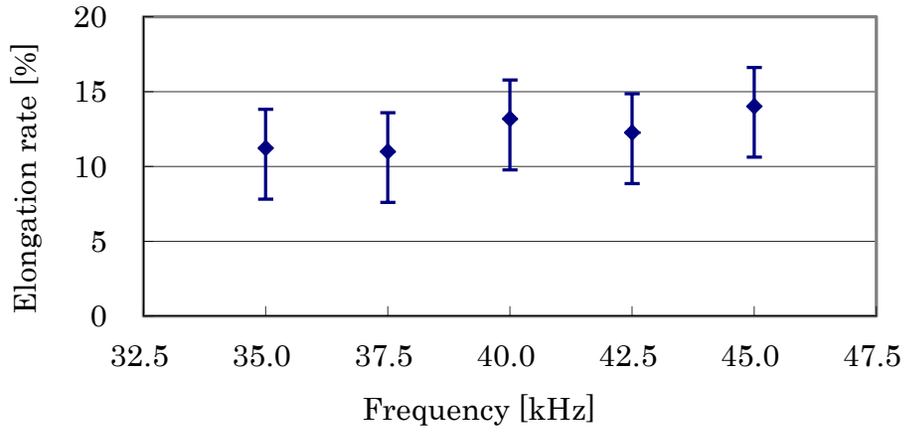

Figure 11. The dependence of elongation rate on frequency

3.3. Dependence of annealing temperature on dielectric material

In this part, the effects of dielectric's material on annealing condition are observed. Figure 12 shows the comparison of the elongation rate with the dielectric substances. This result shows that the elongation rate strongly depends on the dielectric materials. The elongation rate using

BN is higher rate than using SiO_2. According to a comparison of properties of some dielectric materials (SiO_2, Al_2O_3, BN and glass), we acknowledge that dielectric with higher dielectric constants is more effective to reach the annealing temperature as shown in Table 5. Physical characteristics of the dielectric, such as thermal expansion and melting point, are also important. For example, from our experiment the alumina can be suddenly broken with long duration annealing using a water-cooled electrode due to its large thermal expansion. For the best annealing result, boron nitride is an excellent choice for the dielectric material.

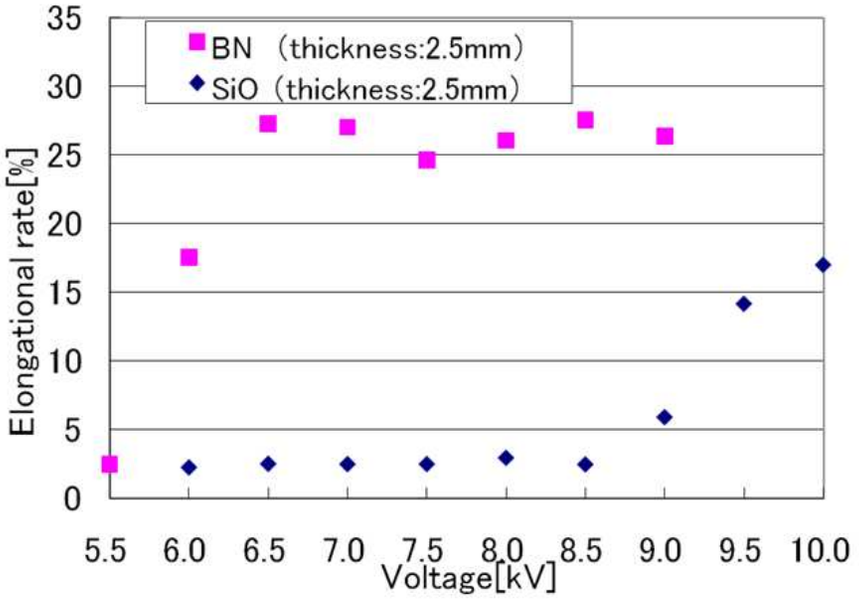

Figure 12. The dependence of elongation rate on dielectric material

Material properties	SiO_2	BN	Al_2O_3	Pyrex Glass
Maximum Temperature (°C)	1713	850	1500	821
Permittivity (F/m)	4.0	6.7	9.5	4.7
Bending strength (Mpa)	105	60.2	310	59.3
Thermal conductivity (W/mK)	1.9	30.98	24	1.005
Thermal expansion (K-1)	8×10^{-6}	0.87×10^{-6}	6.4×10^{-6}	3×10^{-6}

Table 5. Material properties of dielectric

3.4. Dependence of annealing temperature on the thickness of dielectric

Figure 13 shows the dependence of elongation rate on dielectric thickness. This result shows that the annealing effect strongly depends on the dielectric thickness. Compared to the elongation rate, the elongation rate using thin dielectric is higher rate than that using thick ones.

3.5. Dependence of annealing temperature on dielectric size

Figure 14 shows the relation of the elongation rate and the diameter of dielectric. The size of dielectric is weakly affects elongation rate. It is noteworthy that when the copper wire is

driven through the reactor, the chatter motion changes the discharge gap length and heating point on the wire surface and consequently, the annealing result. Moreover, when the thin copper wire is annealed in a wide reactor, discoloration and unevenness occur on the wire surface due to the streamer length density reduction. To obtain a steady discharge state, it is usually necessary to reduce discharge gap length. However, decreasing the reactor gap reduces the discharge volume and consequently, the annealing temperature.

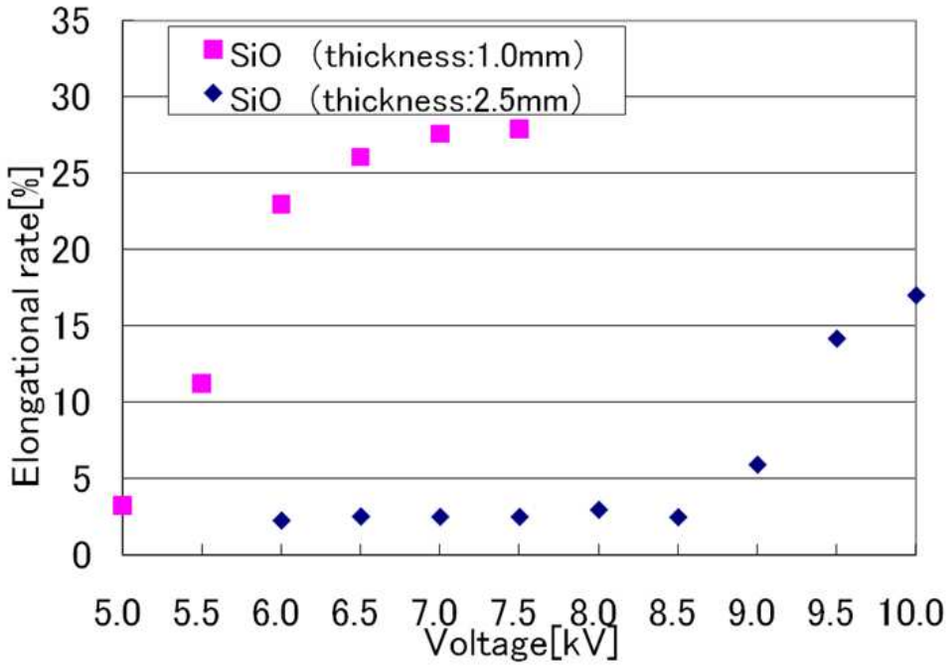

Figure 13. The dependence of elongation rate on dielectric thickness

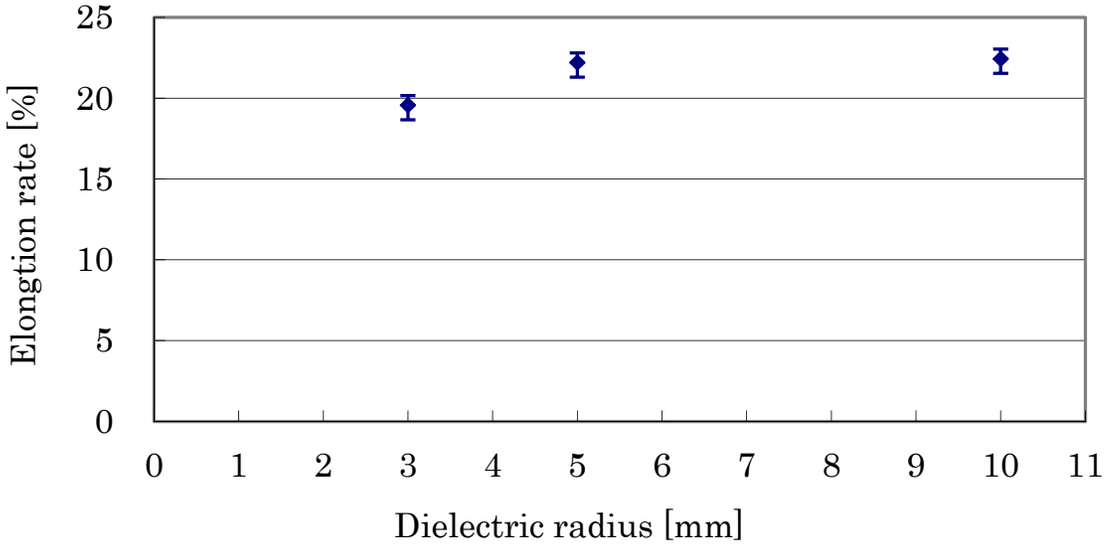

Figure 14. The dependence of elongation rate on dielectric size

4. Equivalent circuit model

In this part, an equivalent circuit model is used to analyze the dependence of the thin copper wire annealing temperature on the dielectric in APDBD. From analysis model, the main factor that determines annealing temperature is the ion bombardment on the wire surface. The average temperature of the thin copper wire in APDBD reactor is calculated as a function of dielectric diameter, dielectric material, applied voltage, ion mass, and gas thermal conductivity. The effect of dielectric on annealing from analysis model is used to compare with that from experiment.

4.1. Discharge mechanism

The moving of electron and ion in the reactor leads to the discharge current behaviors. Figure 15 shows the reflection of discharge current on the applied voltage 9 kV of Al_2O_3 dielectric. At the beginning of the discharge, when increasing the increment of the applied voltage, $dV/dt > 0$, the discharge current crossing the discharge gap increases. The electrons and ions run instantaneously toward anode and cathode and deposit on them to form two space charges. The internal electric field generated by separation of electron and ion space charge. This electric field increases with the increment of applied voltage and is reversely proportional to external electric field. When the incremental applied voltage reaches the peak, $dV/dt = 0$, the discharge current (displacement current) crossing the discharge gap is zero and the internal electric field reaches maximum, the reverse current is formed. When $dV/dt < 0$, the reverse current exists until the applied voltage reaches the local bottom value ($dV/dt = 0$). The process starts again with the same situation when the instant voltage increases again. From experiment, the currents profile of discharge gases is an invariant sine profile and the total current becomes very broad due to the dominant of displacement current. The behavior of voltage-current in the cylindrical APDBD discharge is the same as that of a series RLC circuit.

The discharge characteristics of the annealing system are represented by the total discharge current, which includes the total of displacement current and the conduction current. From Figure 15, the negative current cycle has higher and shaper peak current than that positive one, that leads to the conclusion that the conduction current at negative cycle is higher than that at positive cycle. It is also shown that the phase different between total current waveform and voltage waveform is almost 90°, which indicate that the displacement current takes up large scale value in the total current. The small conduction current in APDBD is because of high resistivity of dielectric. Figure 15 also shows the changing of displacement current (sine shaped profile) and conduction current (narrow peaks) when increasing applied voltage. As shown from the current waveform, in every haft cycle, the waveform has multi peaks and every peak has a sine shape profile during discharge. This characteristic is different from micro-discharge model (contain many very small, short-lived (nanoseconds), many current filaments). In our experiment, the currents profile of all three discharge gases is an invariant sine profile and total current becomes very broad due to the dominant of displacement current. Therefore, the cylindrical APDBD discharge with helium, argon or nitrogen can be modeled by an equivalent series RLC circuit.

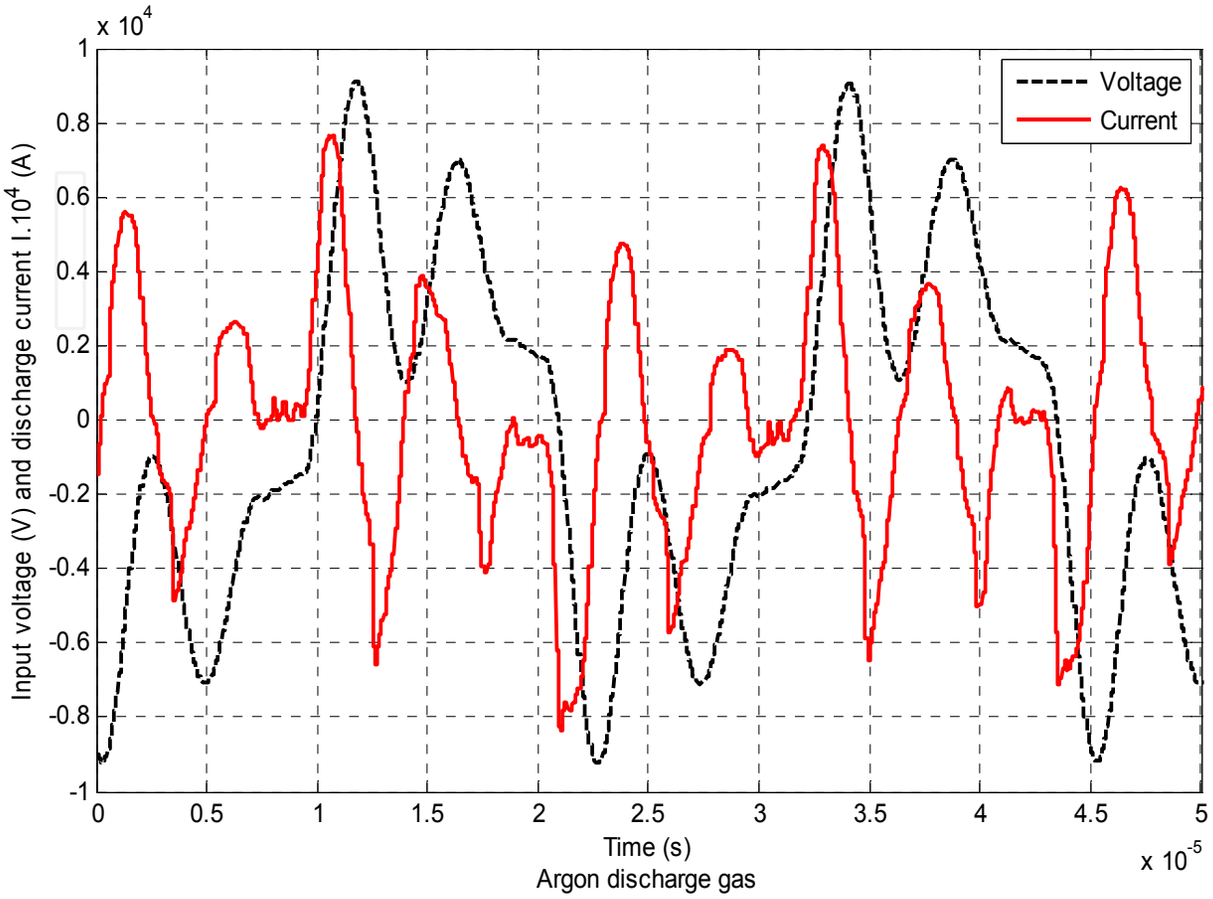

Figure 15. Voltage and discharge current waveform of argon at 8.5 kV

4.2. Equivalent circuit model

Combination between the discharge characteristics of plasma annealing and the reflected physical structure of the plasma reactor, the equivalent circuit model is formed as a RLC circuit in which the total impedance is the combination between series and parallel circuit model. The corresponding main physical part of discharge mechanism shows that plasma reactor can be divided into three parts: (1) dielectric wall, (2) dynamic sheathes and (3) plasma bulk as shown in Figure 16(a). The impedances of dielectric, ionization (Z_p), and non ionization gas capacitance C_g are shown in Figure 16(b). The equivalent circuit model with impedances of dielectric, sheath and plasma bulk is shown in Figure 16(c). In that the impedance of the dielectric is the parallel combination of dielectric capacitance and dielectric heating resistance [32], the impedance of the sheath is the parallel combination of sheath capacitance and ion heating resistance which is presented by ion current in sheath, and the impedance of the plasma is the parallel combination of the R_p (only the ohm heating by streamer is considered) with the cylindrical space capacitance C_p [33]. The diodes, D_a and D_b, are used to specify the sign of the input voltage. The gas capacitance of the reactor before discharging is also connected to the parallel C_g.

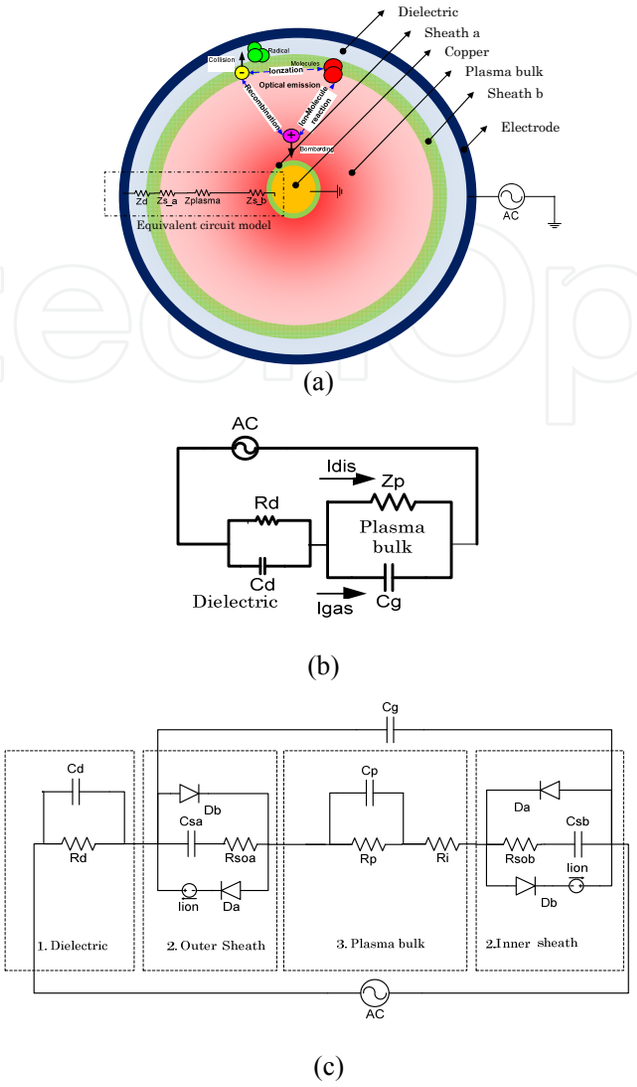

Figure 16. Equivalent circuit model

4.3. The dependence of annealing result on dielectric material

Based on the assumption of the ion heating power, the thin wire temperature from model is [34]

$$T_w = \frac{8r_a l\varepsilon_0\sqrt{\frac{2q}{M}}f\int_0^{\frac{\tau}{2}}\left(\frac{0.84\left(V_{in}(t)-Z_{die}I_{in}(t)\right)\left(\frac{A_b}{A_a}\right)^i}{1+\left(\frac{A_b}{A_a}\right)^i}\right)^{\frac{5}{2}}dt}{9r_s\beta^2\left(\rho C_v v r_a^2+\frac{4\pi\lambda}{\ln\left(\frac{r_c}{r_b}\right)}\right)}+T_0 \quad (4)$$

where $V_{in}(t)$ is the applied voltage, $I_{in}(t)$ is the total discharge current, q is the charge of the ion, M is the ion mass, l is the length of the reactor, and r_a, r_b, r_c and r_s are thin wire radius, the dielectric inner and outer radii and sheath radius, β is a tabulated function of the time-varying ratio r_a/r_s, λ is the discharge gas thermal conductivity, f is the applied voltage frequency, v is the copper wire velocity, T_0 is the copper wire temperature before coming into the plasma reactor, C_v is the specific heat capacity, ϱ is the density, A_a and A_b is the cross-section of thin wire and dielectric, respectivity and T_w is the wire surface temperature. Z_{die} is the dielectric admittance and is a parallel combination of the admittance of the dielectric capacitance Z_d and the dielectric heating R_d,

$$Z_{die} = \frac{R_d Z_d}{R_d + Z_d}. \tag{5}$$

The cylindrical geometry dielectric capacitance Cd is

$$C_d = 2\pi\varepsilon_0 K_d \frac{1}{\ln\left(\frac{r_c}{r_b}\right)}, \tag{6}$$

where k_d is the dielectric permittivity. The dielectric heating R_d is obtained from the power loss in dielectric heating P_d [35],

$$R_d = \frac{dk_d\varepsilon_0 \tan\delta}{2\pi f A_d}, \tag{7}$$

where A_d is the dielectric area, d is the dielectric thickness, tanδ is the loss tangent, and f is the applied voltage frequency.

4.4. Modeling results and discussions

For a typical experimental test, the numerical result is calculated with the same input parameters as in the experiment. Equation (4) is used to calculate the copper wire average temperature in the DBD reactor as a function of the dielectric material parameters. The data in Figure 16 is used as the input current parameter to analyze the effect of the dielectric material and the frequency on the wire temperature.

The plasma annealing system shown in Figure 8 is modeled by an equivalent circuit, as shown in Figure 16 with carrier speed 20m/min, dielectric Al_2O_3. Following Child's law for a collision-less sheath in atmospheric pressure plasma annealing with a high plasma density, the area ratio scaling exponent I = 3. The wire temperature outside of the plasma reactor is assumed to be equal to room temperature (T_0 = 20 °C).

4.4.1. Dependence of annealing temperature on frequency

Figure 17 shows the weakly positive relation between the annealing temperature and the input frequency. When the frequency is increasing from 25 kHz to 40 kHz, the annealing

temperature incrementally increases only 10°C. The comparison this result with experiment result we can see that there are the same. Thus, we estimate that frequency has no effect on the annealing temperature.

4.4.2. Dependence of annealing temperature on dielectric material

Figure 18 shows the dependence of annealing temperature on dielectrics material, glass and aluminum oxide. Simulation result shows that the aluminum oxide dielectric is more effective at reaching the annealing temperature than the glass dielectric. This result also is the same as that from experiment. We can conclude that the dielectrics material affects to annealing and cleaning result. The dielectric material that has higher dielectric constants is more effective to reach the annealing temperature.

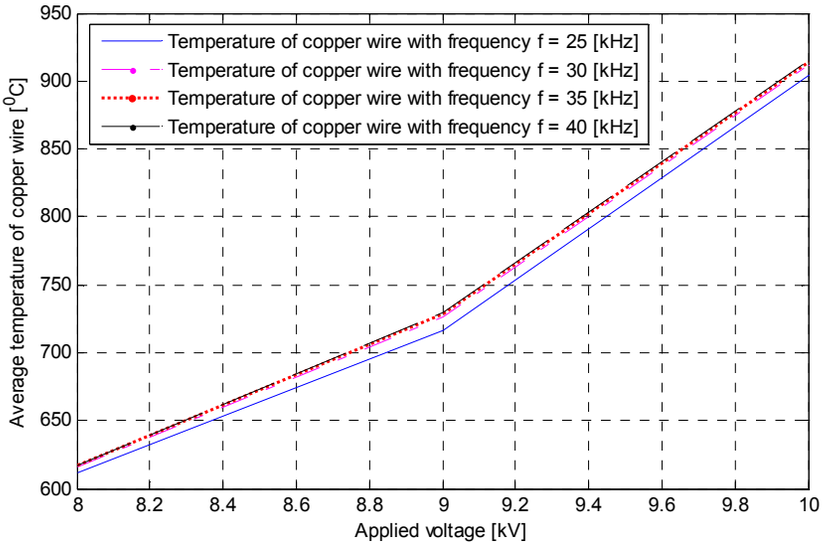

Figure 17. Temperature of copper wire as a function of frequency

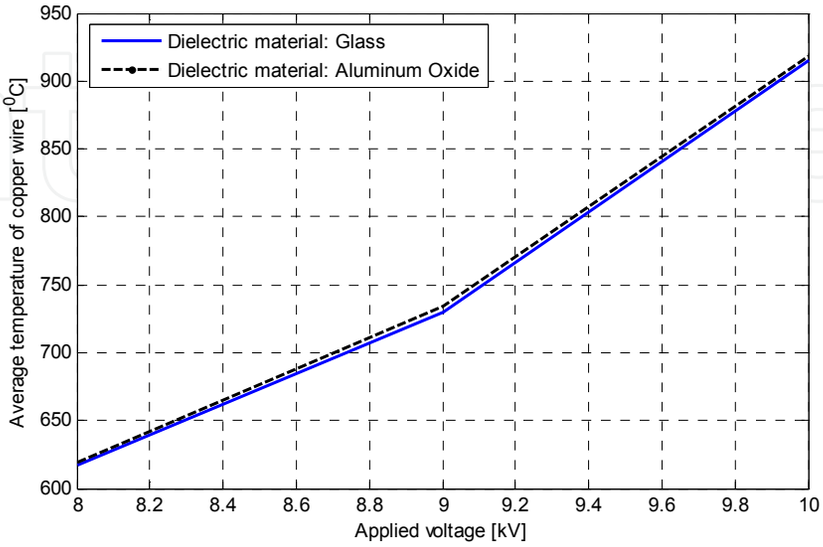

Figure 18. Temperature of copper wire depending on the dielectric material

5. Conclusions

In this chapter, the authors succeeded in setting up the experiment and examining the potential application of dielectric in atmospheric pressure dielectric barrier discharge (APDBD) for annealing and cleaning thin copper wire. The new model of annealing thin copper wire in APDBD also was modeled to RLC equivalent circuit. In conclusion, the dielectric material and dielectric thickness are two parameters which strongly affect to annealing and cleaning thin metallic wire. For optimal annealing conditions, the dielectric with the thinner thickness and the higher dielectric constants is more effective to reach the elongation rate and cleaning surface. Moreover, the dependence of dielectric on frequency of applied power also were considered. The results show that the frequency is slightly effect to dielectric and annealing result.

Author details

N.D. Tran
Energy and Environment Lab., Department of Mechanical Engineering, University of Technical Education Hochiminh City, Thu Duc District, Hochiminh City, Vietnam

T. Kikuchi, N. Harada and T. Sasaki
Plasmadynamics Lab., Department of Electrical Engineering, Nagaoka University of Technology, Kamitomioka, Nagaoka, Niigata, Japan

Acknowledgement

First and foremost, I would like to thank Professor Nobbuhoro HARADA for introducing me to the world of plasmasdynamics. I also would like to thank Associate Professor Takashi Kikuchi and Assistant Professor Toru Sasaki for their generous guidance with worthy advices carrying out this work. I sincerely thank Maeda, Kubo, Kawaii and other colleagues from Plasmadaynamics Lab. for assisting me in experiments and helping me improve my work with their invaluable suggestions.

6. References

[1] K. Maeda, S. Furuya, T. Kikuchi, and N. Harada: 47th AIAA Aerospace Sciences Meeting, Orlando, Florida, (2009), p. 1538.
[2] V. D. Sype: U.S. Patent 6270597B1 (2001).
[3] J. V. O'Gradi: U.S. Patent 2589283 (1951).
[4] Consonen: U.S. Patent 3717745 (1973).
[5] S. Ono, S. Teii, Y. Suzuki, and T. Suganuma: Thin solid films, 518 (2009) 981.
[6] T. Nakamura, C. Buttapeng, S. Furuya, N. Harada: presented at IEEE Int. Conf. Power and Energy, 2008.
[7] M. M. Santillan, A. Vincent, E. Santirso, and J. Amouroux: journal of Cleaner Production, 16 (2008) 198.

[8] C.H. Yi, Y.H. Lee, and G.Y. Yeom: Surf. Coat. Technol. 171 (2003) 237.
[9] T. Nakamura, C. Buttapeng, S. Furuya, N. Harada: Applied Surface Science (2009), doi:10.1016/j.apsusc.2009.05.121.
[10] T. Nozaki, K. Okazaki: Pure Appl. Chem., 78-6(2006) 1157–1172.
[11] Goossens, E. Dekempeneer, D. Vangeneugden, R. Van de Leest and C. Leys: Surface and Coatings Technology , 142-144(2001) 474-481.
[12] G. Borcia C. A. Anderson, N. M. D. Brown: Applied Surface Science, 225- 1-4(2004) 186-197.
[13] J. Park, S. Kyung, G. Yeom: JJAP, 46-38(2007) 942–944.
[14] M. Laroussi: IEEE Trans. Plasma Sci. 30-4(2002)1409-1415.
[15] J. R. Conrad and C. Forest: presented at IEEE Int. Conf. Plasma Science, 1986.
[16] J. R. Conrad, J. Radtke, R. A. Dodd, F. Worzala, and N. C. Tran: J. Appl. Phys. 62 (1987) 4591.
[17] J. L. Shohet: IEEE Trans. Plasma Sci. 19 (1991) 725.
[18] H. J. Hovel and T. F. Kuech: U.S. Patent 4708883 (1987).
[19] R. R. Wei, J. N. Matossian, P. Mikula, and D. Clark: U.S. Patent 5859404 (1999).
[20] S. Choi, S. W. Hwang, and J. C. Park: Surf. Coat. Technol. 142-144 (2001) 300.
[21] D. Wandke, M. Schulze, S. Klingner, A. Helmke, and W. Viol: Surf. Coat. Technol. 200 (2005) 700.
[22] M. Davis, A. Calverley, and R. F. Lever; Appl. Phys., 27 (1956) 195.
[23] K. Marshall and R. Wickham; J. Sci. Instrum., 35 (1958) 121.
[24] J. C. Kelly; J. Sci. Instrum., 36 (1959) 89.
[25] R. E. Haigh and P. H. Dawson; J. Appl. Phys. 12 (1961) 609 doi: 10.1088/0508-3443/12/11/305
[26] G. A. Emmett and M. A. Henry: J. Appl. Phys. 71 (1992) 113.
[27] S. Qin, Z. Jin, and C. Chan: Nucl. Instrum. Methods Phys. Res., Sect. B 114 (1996) 288.
[28] S. Masamune and K. Yukimura: Nucl. Instrum. Methods Phys. Res., Sect. B 206 (2003) 682.
[29] J. O. Rossi, M. Ueda, and J. J. Barroso: IEEE Trans. Plasma. Sci. 28 (2000) 1392.
[30] I. S. Choi, S. W. Hwang, and J. C. Park: Surf. Coat. Technol. 142-144 (2001) 300.
[31] T. Nakamura, C. Buttapeng, S. Furuya, and N. Harada: presented at 2nd IEEE Int. Conf. Power and Energy (PECon 08), 2008, p. 1498.
[32] J. R. Roth and X. Dai: AIAA J. 1203 (2006) 6.
[33] M. A. Lieberman and A. J. Lichtenberg, Principles of Plasma Discharges and Materials Processing (Wiley,New York, 1994), Chap. 4.
[34] Dam N. Tran, Vinh P. Nguyen, Toru Sasaki, Takashi Kikuchi, and Nobuhiro Harada: JJAP, 50(2011) 036202.
[35] E. M. Bazelyan, YU. P. Raizer: Spark Discharge (CRS Press, New Yourk, 1998).